ACCEPTED VERSION

Paul R. Medwell, Peter A.M. Kalt and Bassam B. Dally
Reaction zone weakening effects under hot and diluted oxidant stream conditions
Combustion Science and Technology, 2009; 181(7):937-953

© 2009 Taylor & Francis Group, LLC

This is an Accepted Manuscript of an article published by Taylor & Francis in Combustion Science and Technology on 6 July 2009 available online:
http://dx.doi.org/10.1080/00102200902904138

PERMISSIONS

http://authorservices.taylorandfrancis.com/sharing-your-work/

Accepted Manuscript (AM)

As a Taylor & Francis author, you can post your Accepted Manuscript (AM) on your personal website at any point after publication of your article (this includes posting to Facebook, Google groups, and LinkedIn, and linking from Twitter). To encourage citation of your work we recommend that you insert a link from your posted AM to the published article on **Taylor & Francis Online** with the following text:

*"This is an Accepted Manuscript of an article published by Taylor & Francis in [JOURNAL TITLE] on [date of publication], available online: **http://www.tandfonline.com/**[Article DOI]."*

For example: *"This is an Accepted Manuscript of an article published by Taylor & Francis Group in Africa Review on 17/04/2014, available online: **http://www.tandfonline.com/10.1080/12345678.1234.123456***.

N.B. Using a real DOI will form a link to the Version of Record on **Taylor & Francis Online**.

The AM is defined by the **National Information Standards Organization** as:
"The version of a journal article that has been accepted for publication in a journal."

This means the version that has been through peer review and been accepted by a journal editor. When you receive the acceptance email from the Editorial Office we recommend that you retain this article for future posting.

Embargoes apply if you are posting the AM to an institutional or subject repository, or to academic social networks such as Mendeley, ResearchGate, or Academia.edu.

7 April 2022

http://hdl.handle.net/2440/57145

Full-length article:

Reaction zone weakening effects under hot and diluted oxidant stream conditions

Paul R. Medwell, Peter A. M. Kalt and Bassam B. Dally

School of Mechanical Engineering, The University of Adelaide, S.A. 5005 Australia

Abstract

This paper reports computational results, to complement experimental observations, on the turbulence–chemistry interaction of nonpremixed jet flames issuing into a heated and highly diluted oxidant stream. It is found experimentally that large-scale vortices and flame stretch can lead to spatial thinning and a decrease in OH concentration. This reduction in OH is described as a weakening of the reaction zone. Accompanying reaction zone weakening is also an increase in H_2CO levels. The reduction in reaction rates is most noticeable at low oxidant stream O_2 levels. The heated and low oxygen oxidant conditions typify those of Moderate or Intense Low oxygen Dilution (MILD) combustion. The computational results indicate that the effects of the low oxygen levels of MILD combustion leads to both a reduction in reaction rates and an increase in transport of O_2 across the reaction zone. The relationship between the reaction rate and level of O_2 permeation suggests that a form of partial premixing can occur under MILD combustion conditions. This partial premixing leads to the formation of flame intermediates which contribute to the stabilisation of the flames. The permeation effects are most pronounced at high strain rates, which are commonly encountered in practical MILD combustors.

Key words: Reaction zone weakening, MILD combustion, JHC burner

* Corresponding Author. Tel: +61 (0)8 8303 6941; Fax: +61 (0)8 8303 4367
Email addresses: paul.medwell@adelaide.edu.au (Paul R. Medwell), pkalt@mecheng.adelaide.edu.au (Peter A. M. Kalt), bassam.dally@adelaide.edu.au (Bassam B. Dally).

1 Introduction

Moderate or Intense Low oxygen Dilution (MILD) combustion is a particular combustion regime which involves the strong recirculation of exhaust gases back into the reaction zone (Cavaliere and de Joannon, 2004, Choi and Katuski, 2001, Wünning and Wünning, 1997). The subsequent reduction in localised O_2 concentration leads to a distributed reaction zone, reducing pollutant emissions (notably NO_x) and an increase in nett radiation flux (Cavaliere and de Joannon, 2004, Weber et al., 2000). Application of MILD combustion has been successfully applied in numerous applications, additionally incorporating the use of biomass fuel (HiTACG, 2008). Despite much progress in the application of MILD combustion to practical systems, there remain unresolved issues on the fundamental stabilisation, auto-ignition, and structure of the reaction zone near the jet exit under the hot and diluted conditions (de Joannon et al., 2005, Maruta et al., 2000).

To achieve the very high recirculation rates required for MILD combustion high velocity jets are often used (Cavaliere and de Joannon, 2004). The high strain rate conditions lead to a reduction in turbulence time-scales, coupled with larger chemical time-scales as a result of the low oxygen conditions, these flames are associated with low Damköhler numbers (Katsuki and Hasegawa, 1998). As an extension to this, in a furnace environment MILD combustion has been likened to a well-stirred reactor (WSR) (Plessing et al., 1998, Weber et al., 1999). Based on the concept of attempting to infer MILD combustion from a well-stirred reactor, de Joannon et al. (2000) has attempted to model a WSR with MILD combustion conditions. However as identified in that work the authors acknowledge that a well-stirred reactor is unfeasible for a practical combustor. Furthermore, the interaction between turbulence and chemistry in describing the nature of MILD combustion is expected to

play a significant role (Katsuki and Hasegawa, 1998). The combustion is controlled by both the kinetics and the mixing (Milani and Saponaro, 2001), and so the analogy to a WSR may not always be applicable to practical systems. The importance of both chemical and turbulent timescales has been shown by Galletti et al. (2007) who reported Damköhler numbers near unity in MILD conditions.

To advance the fundamental understanding of practical MILD combustion furnaces beyond WSR theory, there have been efforts to study MILD combustion furnaces on an experimental level (e.g. (Plessing et al., 1998, Szegö et al., 2008)). Through a series of subsequent studies (Coelho and Peters, 2001, Dally et al., 2004, Özdemir and Peters, 2001) using the furnace of Plessing et al. (1998), it has been reported that computational studies qualitatively match the experimental findings, except in the flow-field near the jet and the NO formation. A similar observation was made between the numerical work of Mancini et al. (2002) for the furnace of Weber et al. (2000). The comparisons between the numerical and experimental results from these furnaces highlights that there are aspects of the stabilisation and turbulence–chemistry interaction under MILD combustion conditions which remain unresolved.

To bridge the knowledge gap between the overly simplified WSR theory, and the complex interactions within a furnace environment (even on an experimental level), Dally et al. (2002a,b) reported on the structure of turbulent nonpremixed jet flames issuing into a heated and diluted coflow. This burner configuration, referred to as a jet in hot coflow (JHC) burner, emulates MILD combustion under simplified and well-controlled conditions. These authors used single-point Raman-Rayleigh-LIF diagnostic techniques to simultaneously measure temperature, major and minor species at different locations in these flames. It was found that major changes in the flame structure occur when reducing the oxygen concentration and that, at higher

jet Reynolds number and low oxygen concentration, oxygen leakage from the surroundings is related to local extinction of the flame. Medwell et al. (2007) extended that work by simultaneous imaging of the hydroxyl radical (OH), formaldehyde (H_2CO) and temperature in the same burner, finding evidence of partial premixing in these flames, and localised extinction in the presence of surrounding air.

It has been identified that the flame stabilisation mechanism appears fundamentally different under MILD conditions. Different stabilisation characteristics have been noted in a MILD combustion furnace (Szegö et al., 2007). Under the hot and diluted coflow conditions, in a JHC burner, pre-ignition reactions have been identified upstream of what appear to be lifted flames (Medwell et al., 2008). The presence of flame intermediates (*viz.* OH and H_2CO) in the apparently lifted region of these flames lead to the term *transitional* flames being adopted to describe this phenomenon. In both transitional and attached flames, H_2CO has been detected along the jet centreline (at x/D=7.6), suggesting diffusion of oxygen atoms well into the reaction zone. Further differences in the stabilisation of MILD combustion is evident by noting that the apparent liftoff height decreases with an increase in jet velocity (Medwell et al., 2008). This finding is consistent with the observation in a furnace environment that increasing the jet velocity helped stabilise the jet flame through enhanced mixing (Dally et al., 2004). Furthermore, Mancini et al. (2007) concluded a similar effect of "preconditioning" of the fuel whereby significant mixing occurs prior to the consumption of the fuel.

Using a JHC burner (Dally et al., 2002a,b, Medwell et al., 2007, 2008), this study aims to examine the structure of the reaction zone of a jet in a heated and diluted coflow. Temperature, the hydroxyl radical and formaldehyde are measured instantaneously and simultaneously using planar laser imaging techniques. The hydroxyl radical (OH) is used as a flame marker while the formaldehyde (H_2CO) interme-

diate species is predominant at low temperatures typical of those found in MILD combustion. The product of [OH] and [H_2CO] has also been suggested as an indicator of the formyl (HCO) radical, which is closely related to the heat release rate (Najm et al., 1998).

In this paper we report on the effect of turbulence–chemistry interaction on the reaction zone structure under hot and diluted oxidant stream conditions. Using the same experimental conditions presented in a companion paper (Medwell et al., 2007), a JHC burner is used to emulate MILD combustion. The fuel used is a mixture of natural gas & hydrogen, and issues into a coflow with a 3% O_2 level. Laminar flame calculations are used to complement, and provide additional insight into, the reaction zone structure effects which were observed experimentally.

2 Experimental Details

The MILD combustion burner used in this study is the jet in hot coflow (JHC) burner used previously (Medwell et al., 2007, 2008), and shown in Figure 1. It consists of a central insulated fuel jet (⌀4.6mm) within an annular coflow (⌀82mm) of hot exhaust products from a premixed secondary burner mounted upstream of the jet exit plane. The coflow O_2 level is 3% (volumetric), with an exit temperature of 1100K. The fuel used in the jet is natural gas (92% CH_4) diluted with hydrogen (H_2) in an equal volumetric ratio. The addition of hydrogen reduces the levels of soot (advantageous for laser techniques) and improves flame stability. Addition of H_2 also has implications for the potential use of hydrogen as a supplemental fuel additive. The jet Reynolds number for the experimental data presented in this paper is 15,000.

Laser induced fluorescence (LIF) is used to image OH and H_2CO, and temperature is inferred from Rayleigh scattering measurements. The laser pulses are fired sequentially to reduce interferences on the other systems, with the entire sequence occurring in 300ns to ensure the flow field is effectively frozen with respect to the fluid time scales. The in-plane resolution of all three ICCD cameras is 160μm, after spatial matching. The laser sheet heights were all ∼12mm, of which the central 8mm portion is presented herein. All images are corrected for laser power and profile variations shot-to-shot based on the signal from a laminar slot burner. Description of the experimental details is described in-depth in a previous publication by the authors (Medwell et al., 2007).

3 Laminar Flame Calculations

Laminar flame calculations have been performed to extend the study beyond the available measurements, and shed more light on the structure of the reaction zone and molecular transport. The OPPDIF routine of the Chemkin package is used to compute temperature and species concentration for opposed-flow diffusion flames. For all calculations the GRI-Mech 3.0 mechanism is used. Previous studies have shown the GRI mechanism to provide agreement with experimental measurements of the JHC burner used in this study under similar conditions (Christo and Dally, 2005, Dally et al., 2002a, Kim et al., 2005).

The opposed-flow laminar diffusion flame configuration represents a one-dimensional flame, analogous to the traverse across the well-defined reaction zone from fuel to oxidant. By increasing the velocity of the flow from two facing nozzles, the strain rate imposed on the flame front can be varied. The strain rate quoted throughout most of this paper is the average normal strain rate reported in the OP-

PDIF post-processor output. The use of a laminar, one-dimensional, configuration provided by the OPPDIF models is a well established methodology to enable the role of strain alone to be de-coupled from the more complex turbulent interactions that are observed experimentally.

Three different oxidant stream temperatures and compositions are used for the calculations, as listed in Table 1. The major species concentrations for the experimental conditions used in the previous publication (Medwell et al., 2007) are found from equilibrium calculations based on the coflow inlet flowrates. The oxidant stream temperature is 1100K (to match the measurement from the JHC burner). For comparison, standard air conditions are included as well. The jet composition is an equal molar ratio of CH_4 & H_2 (i.e. the natural gas is assumed pure methane).

Since the coflow oxidant stream consists of combustion products (H_2O and CO_2), the standard definition of mixture fraction is not appropriately defined for calculations based on the mass fraction of H & C (hydrogen & carbon) atoms. A normalised mixture fraction, $\xi^* = (\xi - \xi_{oxi}) / (\xi_{fuel} - \xi_{oxi})$ is used instead, where ξ_{fuel} & ξ_{oxi} refer to the standard definition of mixture fraction at the fuel and oxidant stream boundaries, respectively.

4 Results and Discussion

4.1 Motivation

Figure 2 shows a selection of instantaneous image triplets of OH, H_2CO, and temperature from the JHC burner (repeated from Medwell et al. (2007)). The jet Reynolds number is 15,000 and the coflow O_2 concentration 3% (volumetric). The

147 images are centred at 35mm downstream of the jet exit plane. The corresponding
148 size of each image is 8mm in height and 30mm wide. The jet centreline is marked
149 by the vertical dashed line.

150 Typically, near the jet exit the images do not show evidence of large-scale vor-
151 tices. The images suggest that the reaction zone appears unconvoluted, as shown
152 in Figure 2a. Nonetheless, a proportion of the images do show signs of large-scale
153 vortices, as indicated by convolution of the temperature and/or flame species. As
154 the flow becomes more convoluted and stretched by vortices, the OH images can
155 show a localised decrease in concentration and a spatial thinning. The phenomenon
156 relating to reductions in the OH layer is described as a "weakening" of the flame
157 front, and forms the basis of this paper. An example of a weakened reaction zone is
158 seen in Figure 2b.

159 The interaction of the vortices with the reaction zone intuitively suggests that flame
160 stretch leads to the observed reduction in OH concentration. Over a range of strain
161 rates up to extinction, the laminar flame calculations presented in Figure 3 sug-
162 gest that the peak OH number density does have a dependence on the strain rate.
163 Similarly, the peak temperature is also dependent on the strain rate. The strain rate
164 presented in Figures 3 & 4 is defined as the maximum absolute normal strain rate
165 across the reaction zone. Apparent from Figures 3 & 4 is that the flames in the
166 heated and diluted oxidant conditions can sustain a much higher strain rate be-
167 fore extinction. It is also noted that the OH number density measured is of a similar
168 magnitude to that predicted by the laminar flame calculations presented in Figure 3.

169 For comparison of the strain rate values to turbulent conditions, the scalar dissipa-
170 tion (χ) is determined from the gradient of the mixture fraction (ξ);

$$\chi = 2\mathcal{D}\left(\nabla\xi \cdot \nabla\xi\right) \tag{1}$$

171 The diffusion coefficient ($\mathcal{D}$) is determined from the mole-fraction weighted mean
172 of the mixture averaged diffusion of the fuel (k = CH_4 and H_2) components, defined
173 as;

$$\mathcal{D}_{km} = \frac{1 - Y_k}{\sum_{j \neq k}^{K} X_j / \mathcal{D}_{jk}} \tag{2}$$

174 The binary diffusion coefficients ($\mathcal{D}_{jk}$) are determined based on polynomial fit with
175 temperature provided by the TRANSPORT library of CHEMKIN.

176 For the two heated oxidant streams the approximate maximum scalar dissipation
177 rate prior to extinction is $\sim$1200 s^{-1} for the 3% O_2 and $\sim$6000 s^{-1} for the 9% O_2
178 oxidant. At standard oxidant conditions the peak scalar dissipation of $\sim$150s^{-1} was
179 estimated. These results confirm that MILD combustion can sustain much higher
180 strain/scalar dissipation than under conventional oxidant stream conditions.

181 Experimental measurements of H_2CO show an increase with Reynolds number
182 (Medwell et al., 2007). An increase in H_2CO with strain is also noted in the lam-
183 inar flame calculations presented in Figure 5. H_2CO has also been shown to in-
184 crease with the extent of partial premixing (Mc Enally and Pfefferle, 2000, Med-
185 well et al., 2007). To investigate the possibility of a connection between the increase
186 in H_2CO with strain and partial premixing, the O_2 concentration at the location of
187 peak H_2CO is plotted against strain in Figure 6.

188 Figure 6 suggests a relationship between strain and partial premixing is plausible.
189 Since H_2CO is formed on the fuel-rich side of the reaction zone, the O_2 concentra-

tion at the location of peak H_2CO is indicative of the amount of O_2 which has been transported across the flame front. The molecular transport of O_2 to the fuel-rich side is suggestive of a form of partial premixing, and is seen to increase with the strain rate. The presence of oxygen on the fuel-rich side of the reaction zone has been noted previously in MILD combustion conditions (Kim et al., 2005).

4.2 Formaldehyde Production

The H_2CO production rates have been analysed from laminar flame calculations. For each oxidant stream composition, two strain rate conditions have been chosen to differentiate between low and high strain cases, *viz.* 30 s^{-1} and 200 s^{-1} (averaged normal strain rate, corresponding to maximum absolute normal strain rates of $\sim$50 s^{-1} and $\sim$500 s^{-1}). Previous studies have shown the validity of laminar flame calculations to model these flames when using moderate strain rates, of the order of 30 s^{-1} to 200 s^{-1} (Dally et al., 2002a).

Five main reactions have been found to be responsible for the majority of H_2CO formation and consumption. The key reactions identified are (numbered in accordance with GRI);

$$\begin{aligned}
&\textit{R10:} && \mathrm{O{+}CH_3} &&\rightleftharpoons&& \mathrm{H{+}H_2CO}\\
&\textit{R56:} && \mathrm{H{+}H_2CO\ (+M)} &&\rightleftharpoons&& \mathrm{CH_2OH\ (+M)}\\
&\textit{R58:} && \mathrm{H{+}H_2CO} &&\rightleftharpoons&& \mathrm{HCO{+}H_2}\\
&\textit{R101:} && \mathrm{OH{+}H_2CO} &&\rightleftharpoons&& \mathrm{HCO{+}H_2O}\\
&\textit{R127:} && \mathrm{CH{+}H_2O} &&\rightleftharpoons&& \mathrm{H{+}H_2CO}
\end{aligned}$$

For the 3% O_2 oxidant stream case, Figures 7a & 7b show the production rate of H_2CO plotted against mixture fraction for the five selected reactions at two different strain rates. Reactions R10 and R127 are seen to be the main contributors to H_2CO production. H_2CO production via R10 increases by a factor of ten between the two strain rates considered. In comparison, R127 increases by a factor of three. The increase of H_2CO production as the strain rate is increased is consistent with Figure 5. Accompanying the increase in H_2CO production is also an increase in the consumption rate. Reactions rates for R58 and R101 increase by a factor of five and three, respectively, between the two strain rate cases. Nevertheless, the large increase in the reaction rate of R10 with strain over-compensates for the differences in consumption, leading to the higher H_2CO concentration at the higher strain condition.

The rate of H_2CO production via reaction R10 for the two strain cases under consideration is shown in Figures 8a & 8b. Also shown in these figures are the species relevant to H_2CO production via reaction R10 (*viz.* O and CH_3). A vertical line is included as a reference point at the location of the peak nett H_2CO production rate. At this mixture fraction, it is noted that the O concentration is very low for the low strain case, but is significantly (five fold) higher at the high strain case. This difference in O concentration between the two strain cases, coupled with a two fold increase in CH_3, seems to explain the relative reaction rate of R10.

An increase in the concentration of O at the location of peak H_2CO production seems to be one of the main contributors to the increase of H_2CO with strain. Investigation of reaction rates reveals that the major production of O is from O_2, via reaction *R38*: $\mathrm{H} + \mathrm{O_2} \rightleftharpoons \mathrm{O} + \mathrm{OH}$. The production rate of O via reaction R38, and H & O_2 mole fractions, are also shown in Figures 8a & 8b. It is apparent that the production rate of O at the location of peak nett H_2CO is ten fold greater at

the higher strain rate. This is predominately attributed to a five fold increase in O_2 concentration at the location of peak nett H_2CO between the two strain cases.

It is acknowledged that there are many concurrent processes that occur as the strain rate is increased. Nevertheless, the most significant increase in H_2CO with strain seems to occur via the following path;

$$\mathrm{O_2} \xrightarrow[+\mathrm{H}]{\mathrm{R38}} \mathrm{O} \xrightarrow[+\mathrm{CH_3}]{\mathrm{R10}} \mathrm{H_2CO}$$

The identified pathway relates the increase in H_2CO with strain to an increase in O_2 concentration at the location of peak nett H_2CO production. For these laminar nonpremixed calculations, any O_2 at the location of peak H_2CO must have been transported from the oxidant stream. This transport of O_2 across the reaction zone is likened to partial premixing. The possibility of O_2 existing on the fuel rich side of the reaction zone is not unheard of; in conventional nonpremixed flames O_2 has been measured along the centreline towards the base of an attached flame (McEnally and Pfefferle, 1999).

It is worth noting that both the experimental measurements (Figure 2) and the laminar flame calculations (Figure 8) show a broad H_2CO distribution on the fuel-rich side of the reaction zone. Figure 7 indicates a cessation of significant H_2CO production/consumption above $\xi^* \gtrsim 0.015$, yet high H_2CO concentrations are seen much further into the fuel-rich side (Figure 8). This is strongly indicative of diffusion of H_2CO towards the fuel-rich boundary, and is consistent with previous studies that have shown broad H_2CO distribution is a result of diffusive and convective transport effects (Fotache et al., 1997a,b).

4.3 Transport Effects

As the strain rate increases, it has been demonstrated in this paper that the O_2 concentration on the fuel-rich side of the reaction zone increases. The O_2 level on the fuel-rich side of the reaction zone is controlled by the competition between transport from the oxidant stream and consumption. The nett O_2 consumption rate (i.e. the opposite of production rate) for the two strain cases is shown in Figure 9. For reference purposes, key species mole fractions are also included on this plot. To aid in visualisation, since transport is a physical process, Figure 9 is plotted against distance, instead of mixture fraction. The distance origin is defined as the location of peak HCO; with the fuel-rich side denoted as negative, and the fuel-lean side positive. Although constant between the two plots, the range extends only over the region of interest, and not to the fuel and oxidiser boundaries. As expected, as the strain rate is increased it is apparent there is a spatial compression of the reaction zone. The width of the reaction zone (defined as the distance between the peak OH and H_2CO, as markers of the fuel-lean and -rich peaks, respectively) reduces $\sim$2-fold with the increase in strain.

From Figure 9, the peak O_2 consumption rate is seen to be $\sim$5 times higher at $200s^{-1}$ compared to $30s^{-1}$. The increase in peak consumption rate is due in part to the spatial compression of the physical distances at the higher strain and therefore higher concentrations of the radicals involved. Nevertheless, the integrated O_2 consumption is $\sim$3 times higher at the higher strain rate case.

Despite an increase in the consumption of O_2 with increased strain rate, it has been seen that more O_2 permeates the reaction zone. To compare the differences in transport, the velocity of O_2 for the two strain cases is also included in Figure 9.

The O_2 velocity (v_{O_2}) is defined as the combination of the bulk velocity (u) and the diffusion velocity (V_{O_2}) (Yamada et al., 2003). Using the O_2 velocity, the mass flux transport of O_2 ($j_k = \rho_k Y_k v_k$, with $k = O_2$ (Reaction Design, 1999)) has also been added to Figure 9. It is apparent that the transport flux is significantly higher as the strain rate is increased. Coupled with the spatial compression of the reaction zone with increased strain rate, there is a significant increase in the transport of O_2.

It is therefore apparent that the increased O_2 transport, and reduced spatial scales, associated with the increase in strain rate over-compensate for the increased reaction consumption rates. The result is that more O_2 is capable of penetrating the reaction zone. This observation is consistent with the instantaneous images showing increases in H_2CO near the location of local weakening of the flame front (Figure 2b).

4.4 Comparison between oxidant stream conditions

In the conditions analogous to MILD combustion presented so far, an increase in transport of O_2 across the reaction zone has been observed. To compare these heated and diluted conditions to more conventional flame conditions, Figure 10 presents the same details as shown in Figure 9, but now for a 21% O_2 & 300K oxidant stream. The permeation effects under consideration are primarily prevalent at high strain rates, and so data is presented only for the $a \approx 200 s^{-1}$ condition. The scaling for each of the species is the same between the plots, but the vertical axis range is different to accommodate the differences in the relative intensities. Despite the seven-fold increase in oxidant O_2 concentration, it is apparent that under the conventional oxidant stream conditions there is significantly lower O_2 levels on the fuel-rich side of the reaction zone compared to MILD conditions. In order for

the higher O_2 level in the oxidant stream to be reflected on the fuel-rich side, the transport must also increase compared to the increase in consumption. The peak O_2 consumption rate is 7 times higher at the 21% O_2 level, whereas the O_2 mass flux only increases approximately 4-fold in comparison to the 3% O_2 & 1100K condition. In combination, the increase in consumption relative to transport counteracts the higher oxidant stream O_2 concentration in conventional conditions. In effect, the reaction zone becomes more permeable to O_2 under MILD combustion conditions. The increase in O_2 concentration on the fuel-rich side with a reduction in oxidant O_2 level is consistent with Figure 6.

To bridge the gap between the 3% O_2 & 1100K and 21% O_2 & 300K oxidant, Figure 11 shows the same details again, but for a 9% O_2 & 1100K oxidant stream. As expected (from Figure 6), it is seen in Figure 11 that the O_2 level on the fuel-rich side is significantly reduced at 9% O_2 as compared to the 3% O_2 oxidant stream. The three-fold difference in the O_2 level is accompanied by a three-fold increase in O_2 consumption rate. The increased O_2 level at 9% as compared to 3% leads only to a two-fold increase in O_2 flux. Again, the increase in consumption is greater than the increase in flux, such that the O_2 permeation to the fuel-rich side is less.

It is apparent that the lower the O_2 concentration in the oxidant stream the higher the degree of permeation of O_2 across the reaction zone. The lower reaction rates as a result of the low O_2 conditions associated with MILD combustion therefore lead to a form of partial premixing. These findings suggest that molecular transport and finite rate chemistry effects are essential in order to capture the stability and structure of these flames. The challenge remains, however, to capture the transition from a MILD regime to conventional flames (Christo and Dally, 2005).

4.5 Stabilisation

In the low oxygen & high temperature oxidant stream conditions presented, it has been seen that transport of O_2 across the reaction zone is responsible for an increase in the formation of key flame intermediates (notably H_2CO). As the strain rate is increased, these intermediates continue to be generated. The production of such flame intermediates is responsible for the stabilisation of the reaction.

For flames similar to those presented in the current paper, Medwell *et al.* Medwell et al. (2008) identified flame intermediates and pre-ignition reactions upstream of an apparent liftoff height. Due to the presence of intermediates in what is generally considered the liftoff region, the term "transitional" flames was adopted to describe these unique conditions.

As the velocity (hence strain rate) approaches lift-off, rather than the transitional flames becoming completely lifted, the formation of intermediates continues. It is proposed that in the "lift-off" region a pool of intermediates is produced. These precursors initiate the combustion reaction, and are believe to greatly enhance the stabilisation of the flame. The build-up of a pool of precursors (notably H_2CO) in jet flames in a similar high temperature coflow has been suggested by Gordon et al. (2007).

5 Conclusion

MILD combustion is a promising combustion regime offering simultaneous reductions in emissions and an increase in thermal efficiency. Laminar flame calculations in the low oxygen and high temperature conditions of MILD combustion have been

shown to lead to simultaneous reduction in reaction rates and increased transport across the reaction zone. Enhancing these effects, experimentally it is shown that interaction with large-scale vortices can lead to a spatial thinning of the reaction zone. The turbulence–chemistry interaction under the heated and highly diluted oxidant stream is referred to as reaction zone weakening. The effects of strain is particularly important for MILD combustion since practical combustors typically rely on high velocity jets to achieve the highly diluted conditions.

As the flame-front is stretched at the low oxygen (3% O_2) and high temperature (T_{oxi}=1100K) conditions, reaction zone weakening manifests itself in two ways; the strain effect leads to an increase in H_2CO, and large-scale vortices lead to a reduction in OH concentration. The low O_2 conditions lead to a reduction in reaction rate, that is, a weaker reaction zone (as compared to higher O_2 oxidant stream conditions). When the strain rate is increased, the effects of weakening, combined with a spatial compression of the reaction zone, contribute to a greater degree of O_2 transport across the reaction zone. Therefore, in MILD combustion a form of partial premixing occurs. Large-scale turbulent mixing due to large-scale vortices can lead to a weakening of the flame front. This observation demonstrates the importance of turbulent mixing in the establishment of the MILD combustion regime.

Reaction zone weakening, which leads to a form of partial premixing, may contribute to the stabilisation of the MILD combustion reaction zone. Previous studies have shown that an increase in jet velocity helps stabilise flames under MILD conditions (Dally et al., 2004, Medwell et al., 2008). The partial premixing effects that have been identified provide an increase in the formation of flame intermediates, and thus an improvement in the stabilisation with jet velocity.

Acknowledgments

The authors would like to thank Dr Zeyad Alwahabi for his assistance with this project. The financial support of The University of Adelaide and the Australian Research Council is gratefully acknowledged.

References

A. Cavaliere and M. de Joannon. Mild combustion. *Progress in Energy and Combustion Science*, 30:329–366, 2004.

G.-M. Choi and M. Katuski. Advanced low NO_x combustion using highly preheated air. *Energy Conversion and Management*, 42:639–652, 2001.

F. C. Christo and B. B. Dally. Modeling turbulent reacting jets issuing into a hot and diluted coflow. *Combustion and Flame*, 142:117–129, 2005.

P. J. Coelho and N. Peters. Numerical simulation of a mild combustion burner. *Combustion and Flame*, 124:503–518, 2001.

B. B. Dally, A. N. Karpetis, and R. S. Barlow. Structure of turbulent non-premixed jet flames in a diluted hot coflow. *Proceedings of the Combustion Institute*, volume 29, pages 1147–1154, 2002a.

B. B. Dally, A. N. Karpetis, and R. S. Barlow. Structure of Jet Laminar Non-premixed Flames under Diluted Hot Coflow Conditions. *2002 Australian Symposium on Combustion and The Seventh Australian Flame Days*, Adelaide, Australia, 2002b.

B. B. Dally, E. Riesmeier, and N. Peters. Effect of fuel mixture on moderate and intense low oxygen dilution combustion. *Combustion and Flame*, 137:418–431, 2004.

M. de Joannon, A. Cavaliere, T. Faravelli, E. Ranzi, P. Sabia, and A. Tregossi. Analysis of process parameters for steady operations in methane mild combustion technology. *Proceedings of the Combustion Institute*, volume 30, pages 2605–2612, 2005.

M. de Joannon, A. Saponaro, and A. Cavaliere. Zero-dimensional analysis of diluted oxidation of methane in rich conditions. *Proceedings of the Combustion Institute*, volume 28, pages 1639–1646, 2000.

C. G. Fotache, T. G. Kreutz, and C. K. Law. Ignition of Hydrogen-Enriched Methane by Heated Air. *Combustion and Flame*, 110:429–440, 1997a.

C. G. Fotache, T. G. Kreutz, and C. K. Law. Ignition of Counterflowing Methane versus Heated Air under Reduced and Elevated Pressures. *Combustion and Flame*, 108:442–470, 1997b.

C. Galletti, A. Parente, and L. Tognotti. Numerical and experimental investigation of a mild combustion burner. *Combustion and Flame*, 151:649–664, 2007.

R. L. Gordon, A. R. Masri, S. B. Pope, and G. M. Goldin. Transport budgets in turbulent lifted flames of methane autoigniting in a vitiated co-flow. *Combustion and Flame*, 151:495–511, 2007.

HiTACG. In *7th International Symposium of High Temperature Air Combustion and Gasification*, Phuket, Thailand, 13-16 January 2008.

M. Katsuki and T. Hasegawa. The science and technology of combustion in highly preheated air combustion. *Proceedings of the Combustion Institute*, volume 27, pages 3135–3146, 1998.

S. H. Kim, K. Y. Huh, and B. Dally. Conditional moment closure modeling of turbulent nonpremixed combustion in diluted hot coflow. *Proceedings of the Combustion Institute*, volume 30, pages 751–757, 2005.

M. Mancini, R. Weber, and U. Bollettini. Predicting NO_x emissions of a burner operated in flameless oxidation mode. *Proceedings of the Combustion Institute*, volume 29, pages 1155–1163, 2002.

M. Mancini, P. Schwöppe, R. Weber, and S. Orsino. On mathematical modelling of flameless combustion. *Combustion and Flame*, 150:54–59, 2007.

K. Maruta, K. Muso, K. Takeda, and T. Niioka. Reaction zone structure in flameless combustion. *Proceedings of the Combustion Institute*, volume 28, pages 2117–2123, 2000.

C. S. Mc Enally and L. D. Pfefferle. Experimental study of nonfuel hydrocarbons

and soot in coflowing partially premixed ethylene/air flames. *Combustion and Flame*, 121:575–592, 2000.

C. S. McEnally and L. D. Pfefferle. Experimental Study of Nonfuel Hydrocarbon Concentrations in Coflowing Partially Premixed Methane/Air Flames. *Combustion and Flame*, 118:619–632, 1999.

P. R. Medwell, P. A. M. Kalt, and B. B. Dally. Simultaneous imaging of OH, formaldehyde, and temperature of turbulent nonpremixed jet flames in a heated and diluted coflow. *Combustion and Flame*, 148:48–61, 2007.

P. R. Medwell, P. A. M. Kalt, and B. B. Dally. Imaging of diluted turbulent ethylene flames stabilized on a Jet in Hot Coflow (JHC) burner. *Combustion and Flame*, 152:100–113, 2008.

A. Milani and A Saponaro. Diluted combustion technologies. Technical Report Article Number 200101, IFRF Combustion Journal, February 2001.

H. N. Najm, P. H. Paul, C. J. Mueller, and P. S. Wyckoff. On the adequacy of certain experimental observables as measurements of flame burning rate. *Combustion and Flame*, 113:312–332, 1998.

I. B. Özdemir and N Peters. Characteristics of the reaction zone in a combustor operating at MILD combustion. *Experiments In Fluids*, 30:683–695, 2001.

T. Plessing, N. Peters, and J. G. Wünning. Laseroptical investigation of highly preheated combustion with strong exhaust gas recirculation. *Proceedings of the Combustion Institute*, volume 27, pages 3197–3204, 1998.

Reaction Design. TRANSPORT: Chemkin Collection Release 3.5. User Manual TRA-035-1, 1999.

G. G. Szegö, B. B. Dally, and G. J. Nathan. Stability limits of a parallel jet mild combustion burner system. *Proceedings of the Australian Combustion Symposium*, pages 62–65, 2007.

G. G. Szegö, B. B. Dally, and G. J. Nathan. Scaling of NO_x emissions from a

laboratory-scale mild combustion furnace. *Combustion and Flame*, 154:281–295, 2008.

R. Weber, A. L. Verlaan, S. Orsino, and N. Lallemant. On emerging furnace design methodology that provides substantial energy savings and drastic reductions in CO_2, CO and NO_x emissions. *Journal of the Institute of Energy*, 72:77–83, 1999.

R. Weber, S. Orsino, N. Lallemant, and A. Verlaan. Combustion of natural gas with high-temperature air and large quantities of flue gas. *Proceedings of the Combustion Institute*, volume 28, pages 1315–1321, 2000.

J. A. Wünning and J. G. Wünning. Flameless oxidation to reduce thermal NO-formation. *Progress in Energy Combustion and Science*, 23:81–94, 1997.

E. Yamada, M. Shinoda, H. Yamashita, and K. Kitagawa. Experimental and numerical analyses of magnetic effect on OH radical distribution in a hydrogen-oxygen diffusion flame. *Combustion and Flame*, 135:365–379, 2003.

Oxidant	3% O_2	9% O_2	21% O_2
T_{oxi}	1100K	1100K	300K
O_2	0.03	0.09	0.21
N_2	0.84	0.78	0.79
H_2O	0.10	0.10	0.00
CO_2	0.03	0.03	0.00

Table 1
Oxidant stream temperature and composition (molar basis) used for laminar flame calculations.

List of Figure Captions

Figure 1: Cross-sectional diagram of jet in hot coflow (JHC) burner.

Figure 2: Selection of instantaneous OH, H_2CO, and temperature image triplets (Medwell et al., 2007). Each image 8×30mm. Jet centreline marked with dashed line. Axial location 35mm above jet exit.

Figure 3: Calculated peak OH number density plotted versus maximum absolute strain rate found from laminar flame calculations at various oxidant stream O_2 levels.

Figure 4: Calculated peak temperature plotted versus maximum absolute strain rate found from laminar flame calculations at various oxidant stream O_2 levels.

Figure 5: Calculated peak H_2CO number density plotted versus maximum absolute strain rate found from laminar flame calculations at various oxidant stream O_2 levels.

Figure 6: Calculated O_2 mole fraction (%) at location of peak H_2CO concentration plotted versus maximum absolute strain rate found from laminar flame calculations at various oxidant stream O_2 levels.

Figure 7: H_2CO production rate via major reactions, found from laminar flame calculations. 3% O_2, 1100K oxidant stream for two different strain rates. (Note the different vertical axis scaling.)

Figure 8: Selected species and production rates found from laminar flame calculations. Production rate of H_2CO is shown for reaction R10. Production rate of O is shown for reaction R38. 3% O_2, 1100K oxidant stream for two different strain

rates. Vertical dashed line indicates location of peak H_2CO production rate. (Note the different vertical axis scaling.)

Figure 9: Selected species mole fractions (OH, H_2CO, HCO, O_2), nett O_2 consumption rate (p_{O_2}), O_2 velocity (v_{O_2}), and O_2 mass flux (j_{O_2}), found from laminar flame calculations. 3% O_2, 1100K oxidant stream for two different strain rates.

Figure 10: Selected species mole fractions (OH, H_2CO, HCO, O_2), nett O_2 consumption rate (p_{O_2}), O_2 velocity (v_{O_2}), and O_2 mass flux (j_{O_2}), found from laminar flame calculations. 21% O_2, 300K oxidant stream for strain rate, $a \approx 200 s^{-1}$.

Figure 11: Selected species mole fractions (OH, H_2CO, HCO, O_2), nett O_2 consumption rate (p_{O_2}), O_2 velocity (v_{O_2}), and O_2 mass flux (j_{O_2}), found from laminar flame calculations. 9% O_2, 1100K oxidant stream for strain rate, $a \approx 200 s^{-1}$.

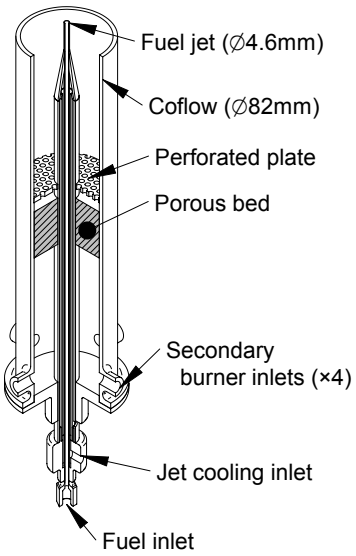

Fig. 1. Cross-sectional diagram of jet in hot coflow (JHC) burner.

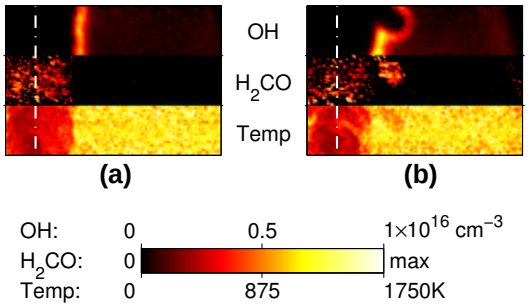

Fig. 2. Selection of instantaneous OH, H_2CO, and temperature image triplets (Medwell et al., 2007). Each image 8×30mm. Jet centreline marked with dashed line. Axial location 35mm above jet exit.

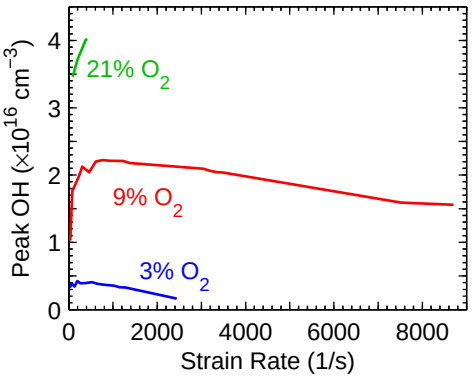

Fig. 3. Calculated peak OH number density plotted versus maximum absolute strain rate found from laminar flame calculations at various oxidant stream O_2 levels.

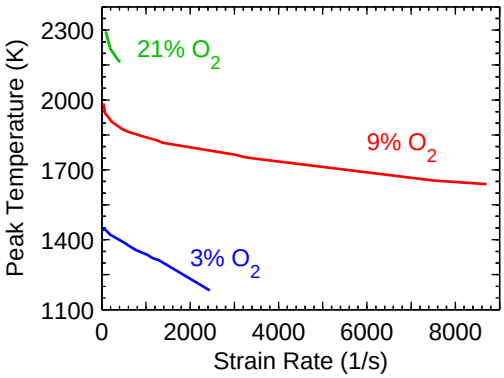

Fig. 4. Calculated peak temperature plotted versus maximum absolute strain rate found from laminar flame calculations at various oxidant stream O_2 levels.

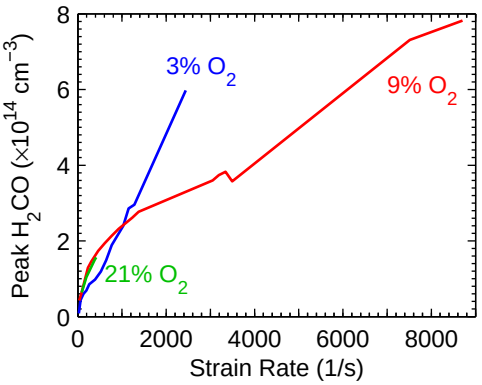

Fig. 5. Calculated peak H_2CO number density plotted versus maximum absolute strain rate found from laminar flame calculations at various oxidant stream O_2 levels.

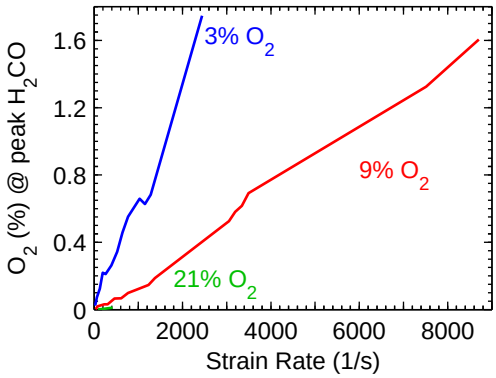

Fig. 6. Calculated O_2 mole fraction (%) at location of peak H_2CO concentration plotted versus maximum absolute strain rate found from laminar flame calculations at various oxidant stream O_2 levels.

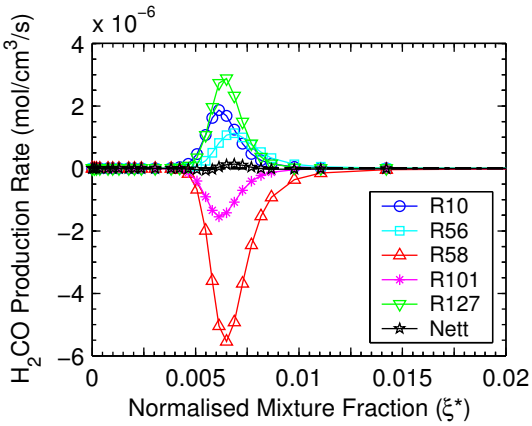

(a) Average strain rate, $a \approx 30 s^{-1}$.

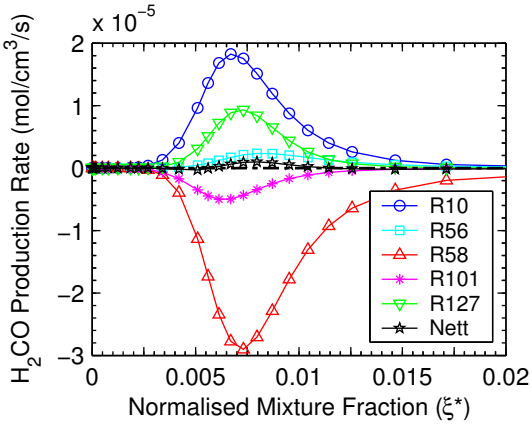

(b) Average strain rate, $a \approx 200 s^{-1}$.

Fig. 7. H_2CO production rate via major reactions, found from laminar flame calculations. 3% O_2, 1100K oxidant stream for two different strain rates. (Note the different vertical axis scaling.)

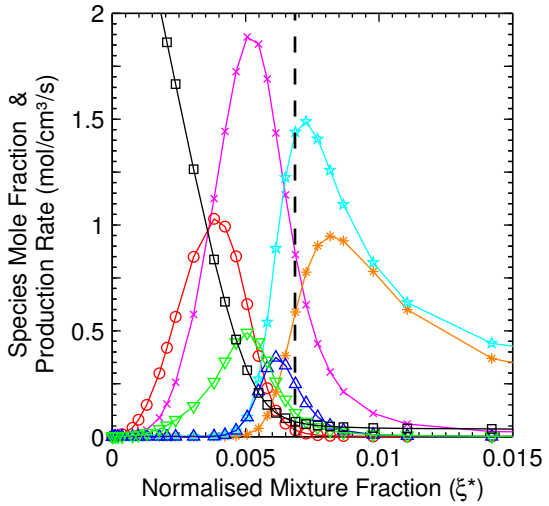

(a) Average strain rate, $a \approx 30 s^{-1}$

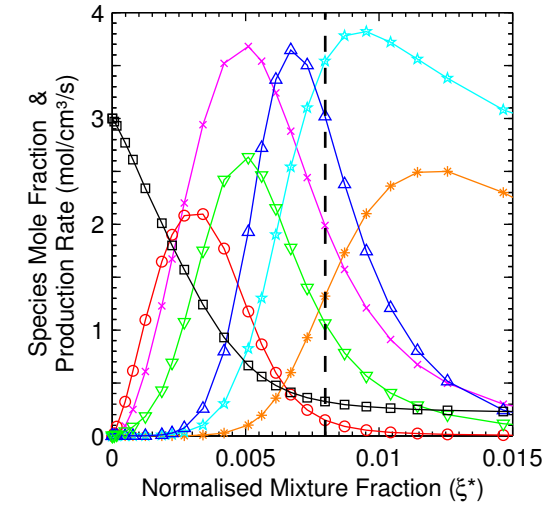

(b) Average strain rate, $a \approx 200 s^{-1}$

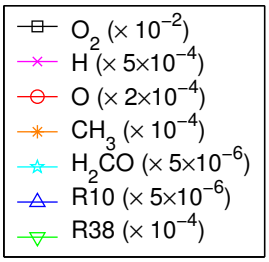

Fig. 8. Selected species and production rates found from laminar flame calculations. Production rate of H_2CO is shown for reaction R10. Production rate of O is shown for reaction R38. 3% O_2, 1100K oxidant stream for two different strain rates. Vertical dashed line indicates location of peak H_2CO production rate. (Note the different vertical axis scaling.)

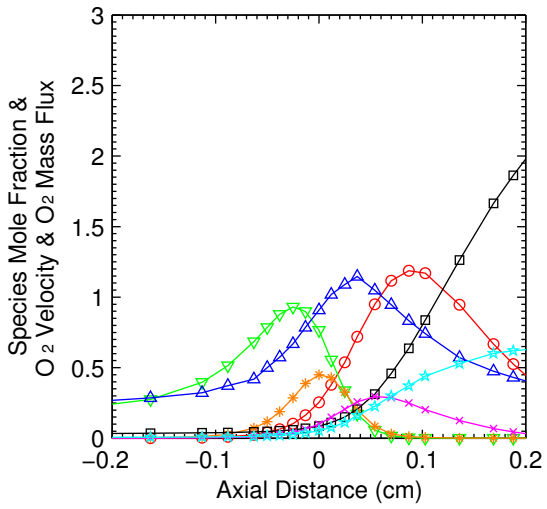

(a) Average strain rate, $a \approx 30 \mathrm{s}^{-1}$.

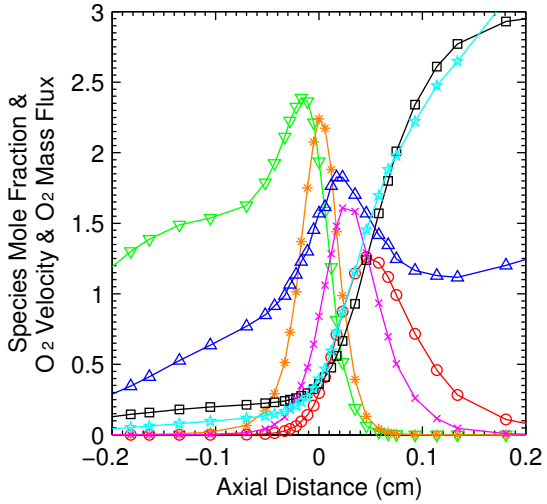

(b) Average strain rate, $a \approx 200 \mathrm{s}^{-1}$.

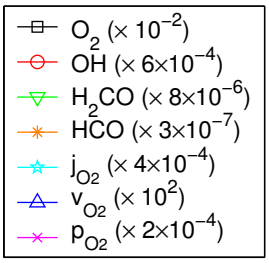

Fig. 9. Selected species mole fractions (OH, H_2CO, HCO, O_2), nett O_2 consumption rate (p_{O_2}), O_2 velocity (v_{O_2}), and O_2 mass flux (j_{O_2}), found from laminar flame calculations. 3% O_2, 1100K oxidant stream for two different strain rates.

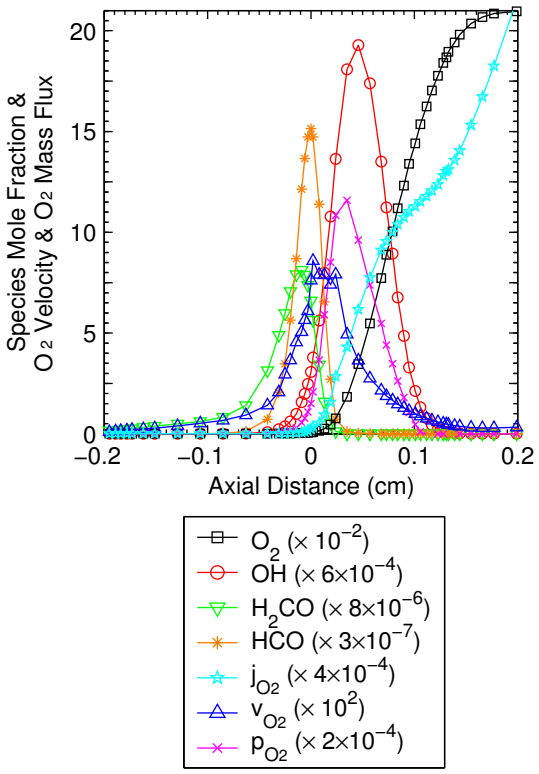

Fig. 10. Selected species mole fractions (OH, H_2CO, HCO, O_2), nett O_2 consumption rate (p_{O_2}), O_2 velocity (v_{O_2}), and O_2 mass flux (j_{O_2}), found from laminar flame calculations. 21% O_2, 300K oxidant stream for average strain rate, $a \approx 200 s^{-1}$.

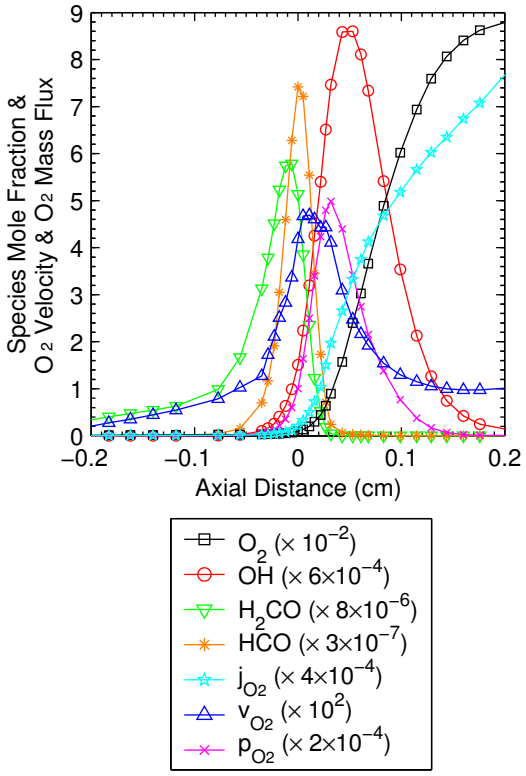

Fig. 11. Selected species mole fractions (OH, H_2CO, HCO, O_2), nett O_2 consumption rate (p_{O_2}), O_2 velocity (v_{O_2}), and O_2 mass flux (j_{O_2}), found from laminar flame calculations. 9% O_2, 1100K oxidant stream for average strain rate, $a \approx 200 s^{-1}$.